Energy & Environmental Science

Accepted Manuscript

This article can be cited before page numbers have been issued, to do this please use: L. Huang, J. Long, H. Chang, Q. Gu, J. Xu, L. Fan, S. Wang, Y. Zhou, W. Wei, X. Wang, P. Liu and W. Huang, *Energy Environ. Sci.*, 2013, DOI: 10.1039/C3EE43289K.

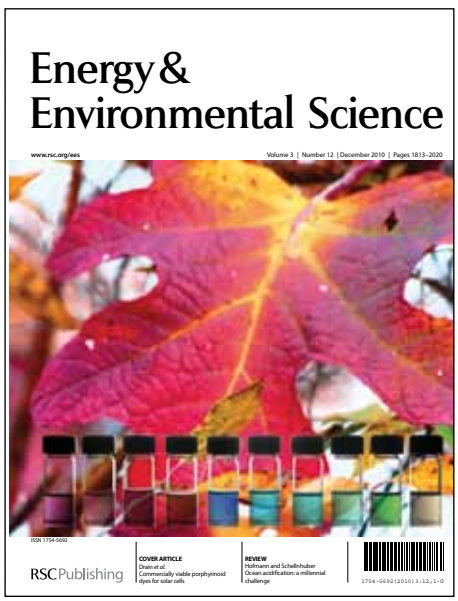

View Article Online
DOI: 10.1039/C3EE43289K

Gold-plasmon enhanced solar-to-hydrogen conversion on the {001} facets of anatase TiO_2 nanosheets

Jinlin Long[a,c,‡,*], Hongjin Chang[b,‡], Quan Gu[a,c], Jie Xu[a], Lizhou Fan[a], Shuchao Wang[c], Yangen Zhou[a], Wei Wei[c], Ling Huang[b,c*], Xuxu Wang[a], Ping Liu[a], and Wei Huang[b*]

[a]*Research Institute of Photocatalysis, Fujian Provincial Key Laboratory of Photocatalysis--State Key Laboratory Breeding Base, Fuzhou University, Fuzhou 350002, China, Fax: 0591-8377912; Tel:0591-83779121; E-mail: jllong@fzu.edu.cn.*
[b]*Institute of Advanced Materials (IAM), NanjingTech University, Nanjing 210009, China, E-mail: iamlhuang@njut.edu.cn; iamwhuang@njut.edu.cn*
[c]*School of Chemical and Biomedical Engineering, Nanyang Technological University, 637457, Singapore. Tel: +65 63168825; E-mail: lhuang@ntu.edu.sg*

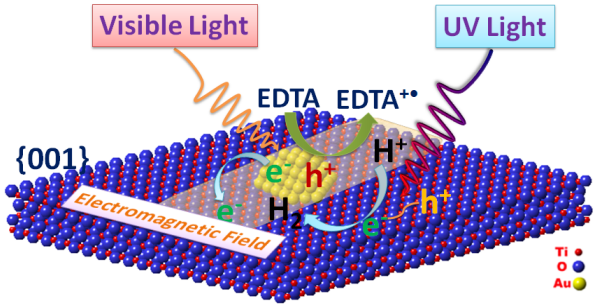

Gold nanoparticles promotes hydrogen production over the {001} facets of anatase nanosheets via the electromagnetic field generated nearby the semiconductor.

View Article Online
DOI: 10.1039/C3EE43289K

Energy & Environmental Science

Cite this: DOI: 10.1039/c0xx00000x

www.rsc.org/xxxxxx

Communication

Gold-plasmon enhanced solar-to-hydrogen conversion on the {001} facets of anatase TiO_2 nanosheets

Jinlin Long[a,c,‡,*], Hongjin Chang[b,‡], Quan Gu[a,c], Jie Xu[a], Lizhou Fan[a], Shuchao Wang[c], Yangen Zhou[a], Wei Wei[c], Ling Huang[b,c*], Xuxu Wang[a], Ping Liu[a], and Wei Huang[b*]

Received (in XXX, XXX) Xth XXXXXXXXX 20XX, Accepted Xth XXXXXXXXX 20XX
DOI: 10.1039/b000000x

A 64-fold improved efficiency of solar-to-hydrogen conversion (SHC) was achieved via exposing Au nanoparticles (NPs) on the {001} facets of anatase TiO_2 nanosheets. The SHC follows a surface plasmon resonance-mediated electron injection mechanism, where Au NPs can not only harvest visible light and convert them to free energetic electrons, but promote the SHC by increasing the electron-hole pair formation rate driven by the electromagnetic field formed nearby the semiconductor.

Broader context

Hydrogen production by Plasmonic photocatalysis is a new exciting field developed recently for solar energy conversion. In this study, we elaborately designed a plasmonic photocatalyst consisting of gold NPs with an average size of 6.0 nm and anatase TiO_2 nanosheets with the exposed (001) facets to achieve a 64-fold improved efficiency of the SHC. The surface plasmon resonance-mediated electron transfer path of the energetic electron generated under visible light (λ>420 nm) irradiation was clearly described by *in situ* ESR technique. More importantly, it was found for the first time that there exists a threshold photon energy of ca. 3.0 eV, corresponding to 413 nm solar photons, for the plasmonic electron transfer over the Au/TiO_2 system. This work represents the latest advances in the area of SHC, also contributes fundamentally to not only the mechanism studies of the SHC, but also the design of novel and high-efficiency photocatalysts, which possess great potentials towards the "green energy" production.

Photocatalyzed solar-to-hydrogen conversion (SHC) at desired efficiency represents one of the most promising alternatives to alleviate our dependence on carbon-based fuels, especially fossil oil, and has received tremendous attention over the past decades. Traditional photocatalysts such as TiO_2, ZnO, and a few binary metal oxides are only able to utilize very limited solar photons (ca. 4%) because of their short wavelength cutoff (large band-gap of > 3.2 eV).[1] Several attempts have been made to engineer their band structures to match the solar electromagnetic spectrum by doping metal and nonmetal ions or creating defects,[2] to localize charge carriers on the surface of the semiconductors by adding dye or inorganic sensitizers,[3] and to construct heterostructures and molecular junctions to improve the charge separation efficiency of photocatalysts,[4] while more work has focused on developing novel photo-functional materials that can harvest visible-light photons and convert them to chemical energy.[5]

It is previously shown that plasmonic metallic nanostructures including Au and Ag nanoparticles (NPs) have the unprecedented ability to concentrate diffuse solar flux into deep-subwavelength volumes and further efficiently convert them to chemical energy.[6] The surface plasmon resonance (SPR) localized at the conduction band of metal nanostructures generally overlaps with the solar spectrum and has been frequently employed to promote the efficiency of a variety of photocatalytic reactions such as degradation of dye pollutants, aerobic oxidation, CO_2 reduction (to hydrocarbon) under visible light irradiation,[7] improvement of the solar-to-electric energy conversion and the photoactivity of electrodes for water splitting.[8] However, only few works have applied the Au SPR effect to study photocatalyzed hydrogen conversion.[9] For example, She et al.[10] compared the plasmonic hydrogen conversion over different Janus Au-TiO_2 nanostructures from isopropyl alcohol/aqueous solution under visible light irradiation and concluded that the local dielectric environment and size of metal nanostructures strongly affect their plasmonic near-fields, and consequently the photocatalytic activity. In fact, metal nanostructures themselves are photocatalytically inert for the hydrogen-conversion reaction. Hydrogen conversion over the plasmonic metal/oxide nanocomposite photocatalysts must be in virtue of the active sites of the oxide semiconductor where the crystal facets, dielectric constants, and crystal structures are pivotal parameters determining the efficiency of the SHC. Among them, the low-indexed crystal facets commonly show high photoreactivities since they have more active sites exposed to the reacting substrates.[11]

However, these efforts are still far away from commercial applications because they don't address the key factors: (1) very diffuse solar flux, (2) high rate of electron-hole recombination and low rate of charge carrier transport in bulk oxide semiconductors, (3) low rate of charge transfer at the semiconductor/liquid interface, and (4) lack of surface sites that allow for the proton reduction to be performed with low activation barriers. Thus, a proper strategy to conquer these obstacles is highly desired to design efficient and robust photocatalysts. Herein, we report Au-plasmon assisted SHC over the reactive {001} facets of anatase TiO_2 nanosheets which can

View Article Online
DOI: 10.1039/C3EE43289K

greatly improve the problems of (2)-(4) and the SHC rate has been improved 64 times by plasmonic photocatalysis.

Anatase TiO_2 nanosheets with the dominant {001} facets were prepared by a solvothermal method.[12] Fig. S1 shows the typical X-ray diffraction peaks of anatase TiO_2 (JCPDS No. 21-1272) and that loaded with varying amount of Au NPs from 0.4 to 3.0 wt% on the {001} facets by the one-plot oleylamine-reduction method.[13] No signal from Au are observed, which maybe because of the low loading amount or high dispersion of Au NPs on TiO_2 surface. The transmission electron microscopy (TEM) image (Fig. 1A) shows that after Au NP loading, the square morphology of anatase TiO_2 is retained (Fig. S2), and a few well-dispersed Au NPs are clearly seen on the {001} planes of TiO_2, at 1.0 wt% loading (denoted as Au/TiO_2-1.0). The high-resolution TEM (HRTEM) image (Fig. 1B) exhibits an interplanar spacing of 0.236 nm corresponding to the {111} crystal plane of face-centered cubic gold, and an interplanar spacing of 0.235 nm indexed towards the {001} direction of the vertical TiO_2 nanosheet. The junction between the {111} crystal plane of Au NP and the {001} facet of anatase TiO_2 is clearly discernable, indicating the perfect contact between each other. The mean size of Au NPs, determined by dark-field scanning TEM (STEM) analysis (Fig. 1C), is 3-8 nm (Fig. 1D), and they grow to 4-10 nm with slightly wider size distribution at 3.0 wt% loading. As expected, the slight increase in particle size doesn't give rise to a significant change in optical absorption and electronic properties (Fig. S3). A broad plasmonic absorption band of Au NPs appears at 400-700 nm[9a] and centered at 534 nm, while the intensity increases with Au loading.

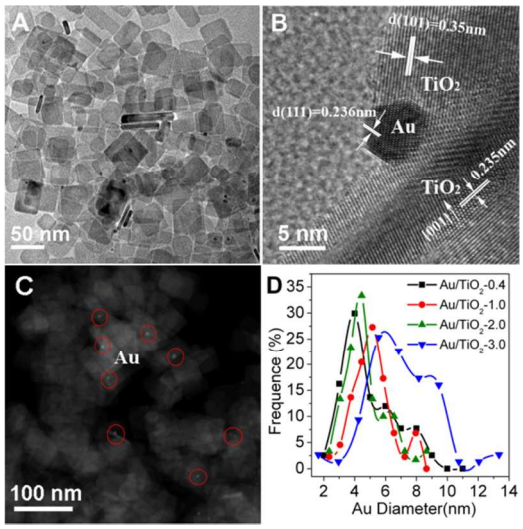

Fig. 1 (A) TEM, (B) HRTEM, and (C) STEM images of Au/TiO_2-1.0. (D) Size distribution of Au NPs on anatase TiO_2 nanosheets determined by dark-field STEM.

Fig. 2A shows the H_2 evolution rates from the aqueous solution of disodium ethylenediaminetetraacetate under artificial solar light irradiation. Fig. S4A gives the results of a typical H_2 conversion where the near-linear dependence on the irradiation time suggests zero-order kinetics for the proton reduction. The lowest H_2 conversion rate over the bare TiO_2 nanosheets is 8.0 μmol g^{-1} h^{-1}, while a 64-fold enhancement (510 μmol g^{-1} h^{-1}) is achieved over the Au/TiO_2-1.0 sample. The H_2 evolution rate decreases significantly upon Au NP loading higher than 1.0 wt%. Under visible-light (≥ 420 nm) excitation, this trend is in parallel with that obtained under solar light irradiation, as shown in Fig. 2B. The H_2 evolution rate increases with Au NP content and reaches a maximum (50.0 μmol g^{-1} h^{-1}) at 1.0 wt% loading. Although the maximal rate of H_2 evolution with visible light irradiation is only one tenth of that obtained with solar light excitation, it is far larger than that (8.5 μmol g^{-1} h^{-1}) of the counterpart prepared by loading the same content of Au NPs on commercial TiO_2 (Fig. S5). More Au NP loading (> 1.0 wt%) results in a distinct decrease in H_2 production rate possibly because of the stronger photon scattering,[6b,14] which is consistent with the result obtained under solar light irradiation. The dependence of H_2 conversion rate on Au content suggests that Au NPs act as visible light sensitizers. It should be noticed that no H_2 is detected over the bare anatase TiO_2 nanosheets because of no absorption in the visible region, whereas a significant jump on H_2 evolution rate is observed and linearly increased with the irradiation time (Fig. S4B), even upon a small amount of Au NP (0.4 wt%) loading. This, together with the plasmonic absorption centered at 534 nm (Fig. S3), indicate that the H_2 evolution is closely related to the localized SPR of Au NPs.

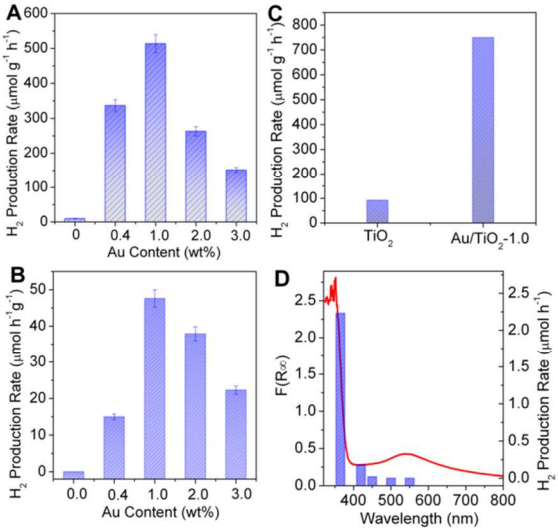

Fig. 2 Photocatalytic H_2 evolution rates of Au/TiO_2 nanosheets with different Au NP contents in the presence of EDTA as a sacrificial electron donor under (A) solar light irradiation, (B) visible light irradiation, and (C) 365 nm light irradiation. (D) Action spectrum of H_2 evolution over the Au/TiO_2-1.0 photocatalyst.

In order to fully elucidate the role of plasmonic Au NPs in the SHC, we further examined the H_2 evolution on bare TiO_2 and Au/TiO_2-1.0 under 365 nm light irradiation. As shown in Fig. 2C, the Au/TiO_2-1.0 exhibits a H_2 evolution rate of 720 μmol g^{-1} h^{-1}, which is 8 times more active than that of the bare TiO_2 nanosheets. The enhancement originates mainly from the action of Au NPs as a cocatalyst. Although the 365 nm light intensity (1.5 W/cm^2) used in this study is greatly higher than that of the solar light (0.33 W/cm^2), the rate enhancement of the former is far lower than that of the later, implying that the SHC over the Au/TiO_2 is predominantly contributed from the plasmonic effect of Au NPs induced by the 365 nm light. Inscrutably, the Au/TiO_2

View Article Online
DOI: 10.1039/C3EE43289K

shows an ill-matched action spectrum of H_2 evolution, consistent with the results reported by Hou et al.[7e] As depicted in Fig. 2D, no H_2 is produced with excitation of a narrowed light flux centered between 480 and 530 nm where a strong plasmonic absorption occurs. The result demonstrates that there is no direct relationship between the SPR intensity and the H_2 evolution rate, which leads to a hypothesis that the plasmonic absorption is unable to create "chemically useful" energetic charge carriers in the Au/TiO_2 composite for H_2 conversion if using a light flux well-matched with the SPR of Au NPs.

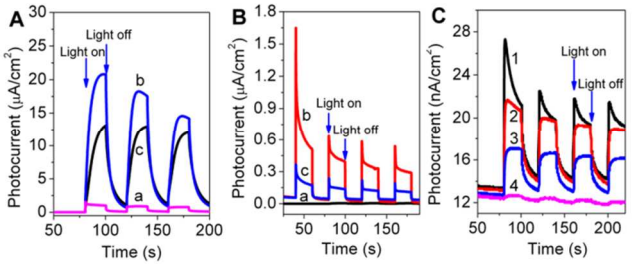

Fig. 3 Short-circuit photocurrent response of (a) TiO_2 nanosheets, (b) Au/TiO_2-1.0, and (c) Au/TiO_2-2.0 in a 0.2 M Na_2SO_4 aqueous electrolyte under (A) solar light and (B) visible light irradiations. (C) Short-circuit photocurrent response of Au/TiO_2-1.0 under irradiation wavelength of (1) 420, (2) 435, (3) 450, and (4) 520 nm.

To confirm this hypothesis, we performed the photo-electrochemical characterization of several representative photocatalysts including bare TiO_2, Au/TiO_2-1.0, and -2.0 to determine the formation and injection transfer of energetic plasmonic electrons. Fig. 3 shows the periodic on/off photocurrent response of such catalysts when irradiated under different lights. Artificial solar light irradiation of bare anatase TiO_2 nanosheets coated on indium tin oxide (ITO) glass reveals a relatively low short-circuit photocurrent, whereas the loading of Au NPs results in a ca. 18-fold increase in the photocurrent (Fig. 3A). This tremendous increase is mainly due to two aspects: i) the predominant plasmonic effect that increases the formation rate of electron-hole pairs over TiO_2; ii) the formation of Schottky barriers among TiO_2-Au-ITO glass, which leads to accelerated transfer of photogenerated electrons from TiO_2 to Au, and finally to ITO. It is important to note that the Au/TiO_2-1.0 exhibits a larger photocurrent than the Au/TiO_2-2.0, in line with the photocatalytic results in Fig. 2A. As such, the visible-light photocurrent density of the Au/TiO_2-1.0 and -2.0 samples (Fig. 3B) also corresponds perfectly to their H_2 evolution rates shown in Fig. 2B. Visible light irradiation of the bare anatase TiO_2 nanosheet electrode doesn't produce any free electrons, which consequently doesn't generate photocurrent, or H_2. The addition of Au NPs generates a significant photocurrent under visible light irradiation, but more Au NPs are deleterious to the photocurrent. Comparison of the photocurrent density finds that the solar-light photocurrent of Au/TiO_2-1.0 is one order of magnitude higher than that produced by visible light irradiation, which also agrees well with the H_2 evolution rate shown in Fig. 2. The photocurrent results obtained under irradiation of different wavelengths further demonstrate the close correlativity of the H_2 conversion rate with the photocurrent. As shown in Fig. 3C, the photocurrent density decreases gradually with increasing radiative wavelength, until to near zero under 520 nm light irradiation. This conclusively demonstrates that plasmonic Au NPs serve as a light-harvesting antenna for the visible-light H_2 conversion and can significantly improve the SHC rate over anatase TiO_2. Thus, we can propose that the plasmon-induced visible light H_2 evolution follows mainly a charge injection mechanism analogous to dye sensitization, where plasmonic-Au NPs absorb visible light and transfer high-energy charge carriers to the anatase TiO_2 nanosheets nearby.[6b,7d]

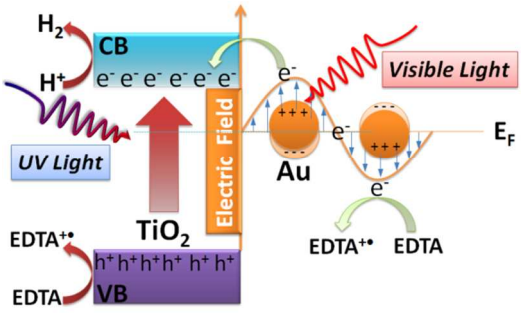

Scheme 1 SPR-mediated electron injection coupled with the electromagnetic near-field for the SHC.

Anatase TiO_2 is characterized by its negative conduction band at ca. -0.50 V versus the normal hydrogen electrode (NHE), while the Fermi energy of Au NPs positioned at ca. +0.45 V versus NHE.[15] Loading of Au NPs on anatase TiO_2 nanosheets can cause the Fermi level of Au and anatase TiO_2 shift to more negative and more positive potentials, respectively, and finally reaches a new Fermi level equilibration. Liu[16] reported a ca. 0.19 eV lowered Fermi level of Au/TiO_2 when Au strip is brought into contact with the TiO_2 surface. Owing to this alignment of the electronic states, the Au/TiO_2 system only allows the transfer of high-energy plasmon electrons of Au NPs across an energy barrier to the conduction band of TiO_2, as depicted in Scheme 1.

There is a threshold photon energy for the plasmonic electron transfer, which can be estimated by $E = E_f - E_{cb} + hC/\lambda$, where E_f and E_{cb} are the Fermi level of plasmonic-metal/semiconductor composite and the conduction band energy of semiconductor, respectively. h is Planck's constant (6.626×10^{-34} J s), C is the speed of light in vacuum (3.0×10^8 m s^{-1}), and λ is the centered wavelength of plasmonic absorption (nanometers). E_{cb} is constant for an indicated semiconductor, while E_f and λ are variables and depend on both plasmonic metal nanostructures and semiconductor. It can be calculated that the threshold energy in the Au/TiO_2 system is equal to ca. 3.0 eV, corresponding to 413 nm solar photons, which well-explains the photoactivity results in Fig. 2D. According to literature,[17] the threshold photon energy may be lowered by 0.2-0.3 eV upon UV light irradiation, because the charge redistribution shifts the Fermi level of Au/TiO_2 to more negative potentials. This will enhance the conversion of more photons in visible light region to energetic electrons, and therefore the rate of H_2 evolution. But the enhancement to H_2 evolution should be limited by simply increasing the injection amount of plasmonic electrons under solar light irradiation. A pivotal contributor, localized electromagnetic field formed by the SPR of supported Au NPs, can't be ignored for the SHC. It has already proved to be able to increase the formation rate of electron-hole pairs of the semiconductor by a few orders of

View Article Online
DOI: 10.1039/C3EE43289K

magnitude.[7b,18] We thus deduce that the SHC follows mainly a SPR-mediated electron injection process coupled with the electromagnetic near-field effect.

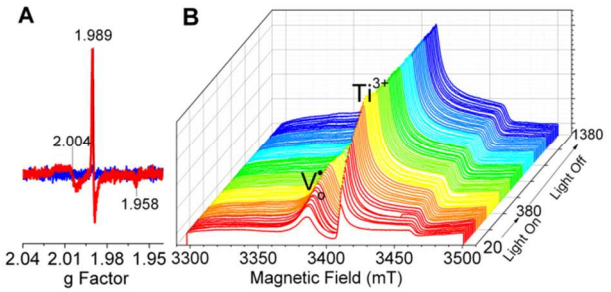

Fig. 4 (A) *In situ* ESR spectra determined at 77 K of the Au/TiO_2-1.0 photocatalyst before (blue) and after (red) visible light irradiation. (B) Integrated ESR spectra of the Au/TiO_2-1.0 photocatalyst as a function of irradiation time.

To prove the SPR-mediated electron-injection from Au NPs to anatase TiO_2 nanosheets under visible light irradiation, we monitored the change of Ti^{3+} species in Au/TiO_2-1.0 by *in situ* electron spin resonance (ESR) at 77 K. There is no signal in the ESR spectrum before light irradiation, but when irradiation is on, a set of signals at g_1 = 1.958, g_2 = 1.989, and g_3 = 1.989 are observed (Fig. 4A), which are unambiguously assignable to surface Ti^{3+} species originated from the electron-trapping of surface-layer Ti^{4+} cations.[19] Moreover, a weak ESR line appears at g = 2.004, characteristic of single electron trapped oxygen vacancies ($V^{\bullet}_o$).[20] Interestingly, the integrated ESR line intensity of $V^{\bullet}_o$ and Ti^{3+} exponentially increases with the irradiation time (Fig. 4B). After 3 min irradiation, the ESR intensity of $V^{\bullet}_o$ reaches a plateau (Figs. 4B and S6), while that of the Ti^{3+} continue to increase exponentially, indicating that there is no relationship between the two ESR signals. Upon light off, a gradual decrease in the intensities of both ESR signals are observed and slowly return to the starting point. It appears that the decay rate of the g = 1.989 line is significantly larger than that of the g = 2.004 line (Fig. S6). This implies that the plasmonic electrons are shallow-trapped on surface Ti^{4+} and thus is easier to be released. Moreover, the surface Ti^{4+} trapped electrons are not paired with single electron-trapped oxygen vacancies, but recombined with holes residing at Au NPs upon light off. These results directly confirm the SPR-mediated electron injection process.

Conclusions

In summary, we have proved that 3-8 nm Au NPs can not only create electric fields nearby the semiconductor photocatalyst to improve the rate of electron-hole pair formation, but also act as photo-sensitizer to harvest visible photons and convert them to electric energy, which imparts the bifunctional Au/TiO_2 nanocomposite excellent photoactivity for the SHC. This work clearly reveals the SPR-mediated electron injection process coupled with electromagnetic near-field for the SHC, which should possesses great potential in developing novel plasmonic photocatalysts.

Acknowledgements

This work was financially supported by the NSFC (Grants Nos. 21373051, 21003021, 21173044 and U1033603), the Science and Technology Project of Education Office of Fujian Province of P. R. China (JA12017), and National Basic Research Program of China (973 Program, No. 2012CB722607). LH thanks the financial support from NTU Start-Up Grant, the Tier 1 Grant (RG20/09) from Ministry of Education (Singapore), and the research grant from the "Jiangsu Specially-Appointed Professors Program", China

Notes and references

[a] *Research Institute of Photocatalysis, Fujian Provincial Key Laboratory of Photocatalysis--State Key Laboratory Breeding Base, Fuzhou University, Fuzhou 350002, China, Fax: 0591-8377912; Tel:0591-83779121; E-mail:* jllong@fzu.edu.cn. *Personal URL:* http://chem.fzu.edu.cn/szdw/teacherinfo.aspx?id=40
[b] *Institute of Advanced Materials (IAM), NanjingTech University, Nanjing 210009, China, E-mail:* iamlhuang@njut.edu.cn; iamwhuang@njut.edu.cn
[c] *School of Chemical and Biomedical Engineering, Nanyang Technological University, 637457, Singapore. Tel: +65 63168825; E-mail:* lhuang@ntu.edu.sg

† Electronic Supplementary Information (ESI) available: [*Detailed synthesis procedures, TEM, XRD, UV-vis DRS, ESR data, and photocatalytic activity as a function of irradiation time*]. See DOI: 10.1039/b000000x/

‡ Footnotes should appear here. These might include comments relevant to but not central to the matter under discussion, limited experimental and spectral data, and crystallographic data.

1 A. L. Linsebigier, G. Lu, J. T.Yates Jr, *Chem. Rev.* 1995, **95**, 735.
2 J. Zhang, Y. Wu, M. Xing, S. A. K. Leghai, S. Sajjad, *Ener. Environ. Sci.* 2010, **3**, 715.
3 S. G. Kumar, L. G. Devi, *J. Phys. Chem. A* 2011, **115**, 13211; W. R. Duncan, O. V. Prezhdo, *Ann. Rev. Phys. Chem.* 2007, **58**, 143.
4 Q. Gu, J. Long, Y. Zhou, R. Yuan, H. Lin, X. Wang, *J. Catal.* 2012, **289**, 88; Q. Gu, J. Long, L. Fan, L. Chen, L. Zhao, H. Lin, X. Wang, *J. Catal.* 2013, **303**, 141; N. Wu, J. Wang, D.N. Tafen, H. Wang, J.-G. Zheng, J.P. Lews, X. Liu, S.S. Leonard, A. Manivannan, *J. Am. Chem. Soc.* 2010, **132**, 6679; J. Tian, Y. Sang, G. Yu, H. Jiang, X. Mu, H. Liu, *Adv. Mater.* 2013, **25**, 5075; J. Tian, Y. Sang, Z. Zhao, W. Zhou, D. Wang, X. Kang, H. Liu, J. Wang, S. Chen, H. Cai, H. Huang, *Small* 2013, DOI: 10.1002/smll.201202346; W. Zhou, Z. Yin, Y. Du, X. Huang, Z. Zeng, Z. Fan, H. Liu, J. Wang, H. Zhang, *Small* 2013, **9**, 140; W. Zhou, G. Du, P. Hu, G. Li, D. Wang, H. Liu, J. Wang, R.I. Boughton, D. Liu, H. Jiang, *J. Mater. Chem.* 2011, **21**, 7937; W. Zhou, H. Liu, J. Wang, D. liu, G. Du, J. Cui, *ACS Appl. Mater. Interfaces* 2010, **2**, 2385.
5 A. Kubacka, M. Fernández-García, G. Colón, *Chem. Rev.* 2012, **112**, 1555; J. Long, S. Wang, Z. Ding, S. Wang, Y. Zhou, L. Huang, X. Wang, *Chem. Commun.* 2012, **48**, 11656. Z. Zhang, J. Long, L. Yang, W. Chen, W. Dai, X. Fu, X. Wang, *Chem. Sci.* 2011, **2**, 1826.
6 J. A. Schuller, E. S. Barnard, W. Cai, Y. C. Jun, J. S. White, M. L. Brongersma, *Nat. Mater.* 2010, **9**, 193; S. Linic, P. Christoper, D. B. Ingram, *Nat. Mater.* 2011, **10**, 911.
7 W. Hou, Z. Liu, P. Pavaskar, W. H. Hung, S. B. Cronin, *J. Catal.* 2011, **277**, 149; D. Tsukamoto, Y. Shiraishi, Y. Sugano, S. Ichikawa, S. Tanaka, T. Hirai, *J. Am. Chem. Soc.* 2012, **134**, 6309; Y. Pan, S. Deng, L. Polavarapu, N. Gao, P. Yuan, C. H. Sow, Q.-H. Xu, *Langmuir* 2012, **28**, 12304; S. Zhu, S. Liang, Q. Gu, L. Xie, J. Wang, Z. Ding, P. Liu, *Appl. Catal. B: Environ.* 2012, **119-120**, 146; W. Hou, W. H Hung, P. Pavaskar, A. Goeppert, M. Aykol, S. B. Cronin, *ACS Catal.* 2011, **1**, 929; S. K. Cushing, J. Li, F. Meng, T. R. Senty, S. Suri, M. Zhi, M. Li, A. D. Bristow, N. Wu, *J. Am. Chem. Soc.* 2012, **134**, 15033.
8 I. Thomann, B. A. Pinaud, Z. Chen, B. M. Clemens, T. F. Jaramillo, M. L. Brongersma, *Nano Lett.* 2011, **11**, 3440; Z. Liu, W. Hou, P. Pavaskar, M. Aykol, S. B. Cronin, *Nano Lett.* 2011, **11**, 1111; D. B. Ingram, S. Linic, *J. Am. Chem. Soc.* 2011, **133**, 5202; J. Lee, S.

View Article Online
DOI: 10.1039/C3EE43289K

Mubeen, X. Ji, G. D. Stucky, M. Moskovits, *Nano Lett*. 2012, **12**, 5104.

9 J.-J. Chen, J. C. S. Wu, P. C. Wu, D. P. Tsai, *J. Phys. Chem. C* 2011, **115**, 210; H. Yuzawa, T. Yoshida, H.Yoshida, *Appl. Catal. B: Environ.* 2012, **115-116**, 294; A. Tanaka, S. Sakaguchi, K. Hashimoto, H. Kominami, *Catal. Sci. Technol.* 2012, **2**, 907.

10 Z. W. She, S. Liu, M. Low, S.-Y. Zhang, Z. Liu, A. Mlayah, M.-Y. Han, *Adv. Mater.* 2012, **24**, 2310.

11 J. Pan, G. Liu, G. Q. Lu, H.-M. Cheng, *Angew. Chem. Int. Ed.* 2011, **50**, 2133.

12 X. Han, Q. Kuang, M. Jin, Z. Xie, L. Zheng, *J. Am. Chem. Soc.* 2009, **131**, 3152.

13 M. Aslam, L. Fu, M. Su, K. Vijayamohanna, V. P. Dravid, *J. Mater. Chem.* 2004, **14**, 1795.

14 N. Naseri, M. Amiri, A. Z. Moshfegh, *J. Phys. D: Appl. Phys.* 2010, **43**, 105405.

15 X. Fu, J. Long, X. Wang, D. Y. C. Leung, Z. Ding, L. Wu, Z. Zhang, Z. Li, X. Fu, *Int. J. Hydrogen Energy* 2008, **33**, 6484.

16 Z.-P. Liu, X.-Q. Gong, J. Kohanoff, C. Sanchez, P. Hu, *Phys. Rev. Lett.* 2003, **91**, 266012.

17 M. Jakob, H. Levanon, P. V. Kamat, *Nano Lett.* 2003, **3**, 353; V. Subramanian, E. E. Wolf, P. V. Kamat, *J. Am. Chem. Soc.* 2004, **126**, 4943.

18 J. Lee, T. Javed, T. Skeini, A. O. Govorov, G. W. Bryant, N. A. Kotov, *Angew. Chem. Int. Ed.* 2006, **45**, 4819.

19 Y. Nakaoka, Y. Nosaka, *J. Photochem. Photobio. A: Chem.* 1997, **110**, 299; Z. Zhang, X. Wang, J. Long, Q. Gu, Z. Ding, X. Fu, *J. Catal.* 2010, **276**, 201; C. P. Kumar, N. O. Gopal, T. C. Wang, M.-S. Wong, S. C. Ke, *J. Phys. Chem. B* 2006, **110**, 5223.

20 J. Zhang, Z. Jin, C. Feng, L. Yu, J. Zhang, Z. Zhang, *J. Solid State Chem.* 2011, **184**, 3066.,